Journal of Sound and Vibration 331 (2012) 4919–4939

Contents lists available at SciVerse ScienceDirect

Journal of Sound and Vibration

journal homepage: www.elsevier.com/locate/jsvi

Vibration signal models for fault diagnosis of planetary gearboxes

Zhipeng Feng [a], Ming J. Zuo [b,*]

[a] School of Mechanical Engineering, University of Science and Technology Beijing, Beijing 100083, China
[b] Department of Mechanical Engineering, University of Alberta, Edmonton, AB, Canada T6G 2G8

ARTICLE INFO

Article history:
Received 25 June 2011
Received in revised form
21 April 2012
Accepted 31 May 2012
Handling Editor: I. Trendafilova
Available online 7 July 2012

ABSTRACT

A thorough understanding of the spectral structure of planetary gear system vibration signals is helpful to fault diagnosis of planetary gearboxes. Considering both the amplitude modulation and the frequency modulation effects due to gear damage and periodically time variant working condition, as well as the effect of vibration transfer path, signal models of gear damage for fault diagnosis of planetary gearboxes are given and the spectral characteristics are summarized in closed form. Meanwhile, explicit equations for calculating the characteristic frequency of local and distributed gear fault are deduced. The theoretical derivations are validated using both experimental and industrial signals. According to the theoretical basis derived, manually created local gear damage of different levels and naturally developed gear damage in a planetary gearbox can be detected and located.

1. Introduction

Compared with fixed shaft gearboxes, planetary gear systems can provide a larger transmission ratio in a more compact package and they are useful for machinery with a high output power requirement. However, due to their heavy load and tough working environment, they are subject to severe wear and impact damage of key components including gears, shafts, and bearings. A failure of the gearbox may cause shutdown of the entire train and result in major economic losses. Therefore, planetary gearbox diagnosis is an important research topic.

In order to diagnose faults of planetary gearboxes, researchers have proposed several methods [1]. For example, McFadden [2,3] and Samuel and Pines [4] generalized the well known time domain averaging method, and respectively proposed the vibration separation method of planet and sun gears. Williams and Zalubas [5] applied Wigner–Ville distribution to detecting faults in helicopter planetary gearboxes. Samuel and Pines [6] proposed constrained adaptive lifting method to analyze individual tooth mesh waveforms in order to detect the presence of damage in helicopter transmissions. Recently, Bartelmus and Zimroz [7,8] found that a planetary gearbox in bad condition is more susceptible to load than in good condition. Based on this finding, they proposed an indicator for vibration condition monitoring of planetary gearbox under nonstationary conditions, which is the linear dependence between the meshing frequency amplitude and the operating condition. Although these works contribute to fault diagnosis of planetary gearboxes, the spectral characteristics of vibration signal still deserve further investigation, because it is not only helpful to detect but also useful to locate gear fault of planetary gearboxes.

* Corresponding author. Tel.: +1 780 492 4466; fax: +1 780 492 2200.
E-mail address: ming.zuo@ualberta.ca (M.J. Zuo).

0022-460X/$ - see front matter © 2012 Elsevier Ltd. All rights reserved.
http://dx.doi.org/10.1016/j.jsv.2012.05.039

Planetary gearbox vibration signals have more complicated spectral components than fixed shaft gear systems. In planetary gearboxes, there are ring gears, sun gears, and planet gears. Usually, the ring gear is stationary, a sun gear rotates around a fixed center, and planet gears not only spin around their own centers but also revolve around the center of the sun gear. The planet gears mesh simultaneously with both the sun gear and the ring gear. Due to these complicated gear motions, the vibration signals generated by planetary gearboxes are more complex than those by fixed shaft gearboxes. In addition, the planet phasing relationship (which is dependent on the number of planets, planet position angles, and the number of teeth of each gear) also adds complexity to vibration signals.

Usually, sensors are fixed on the gearbox casing to collect vibration signals. The relative position of both sun–planet and planet–ring meshing locations with respect to the sensors are time-varying, resulting in amplitude modulation (AM) effect on the sensor perceived signals. This effect further increases the signal complexity.

McFadden and Smith [9], McNames [10], and Mosher [11] studied the spectral structure of planetary gearbox vibration signals, and found that the vibration signal spectrum is typically asymmetric, but they did not consider factors like the frequency modulation (FM) effect, to model the signal. Inalpolat and Kahraman [12] proposed a mathematical model to describe the vibration signal sidebands of planetary gearboxes. They considered configuration parameters such as the number of planets, planet position angles, and the number of gear teeth, and accordingly divided planetary gearboxes into five categories which exhibit distinct sideband behavior from one another in terms of spectral amplitude and frequencies. They took into account of the AM effect caused by the carrier rotation, but neglected the frequency modulation caused by time variation of meshing stiffness or gear damage. Thus, their model is useful to investigate the vibration signal of normal planetary gearboxes, but may not be very powerful to reveal the characteristics of faulty ones. Later, Inalpolat and Kahraman [13] considered the FM effect due to manufacturing errors, and proposed a model from the viewpoint of gear dynamics. This improved dynamic model is good for predicting the sidebands of planetary gear systems due to distributed gear errors. But they did not give explicit equations of the signal spectrum. Meanwhile, manufacturing errors are inevitable even for normal gears. Thus, these research results still need further improvements for practical applications.

In applications, gear faults usually result from local damage on gear tooth surface like pitting, chipping, spalling, and cracking. The vibration signals induced by such local damage will exhibit spectral features that are different from those caused by the manufacturing errors. Hence, we need to investigate the spectral characteristics of planetary gearbox vibration signals with local damage for diagnosis purpose. After a long term running, a local damage usually evolves and ultimately becomes a distributed damage across all the gear teeth. Therefore, we need also to clearly understand the spectral structure of planetary gearbox vibration signals with distributed damage.

Spectral analysis is very popular in the field of machinery fault diagnosis. A thorough understanding of the spectral structure of planetary gearbox vibration signals and of the fault symptoms of each type of gear (sun, planet and ring) would enable more effective fault diagnosis via spectral analysis. However, according to our best knowledge and extensive literature search, we have not found any reports giving explicit equations to describe the spectral structure of planetary gearbox vibration signals, in terms of both the frequency components and their amplitudes, nor giving explicit equations to calculate the characteristic frequency of each type of gear in planetary gearboxes. The lack of knowledge on the spectral structure and gear fault symptoms is a bottle neck issue hindering effective fault diagnosis of planetary gearboxes via spectral analysis.

To address the bottle neck issue, we did the research work described in this paper, and made two major contributions: (1) we considered all the main factors in modeling planetary gearbox vibration signals, including the amplitude modulation and frequency modulation (AMFM) effects caused by both the gear damage and the periodical changes in working conditions (like running speed and load), and the AM effect due to time varying vibration transfer paths. We give explicit equations for modeling planetary gearbox vibration signals, and explicit equations of the corresponding Fourier transform describing the spectral structure in terms of both frequency components and their amplitudes. (2) We give explicit equations to calculate the characteristic frequency of each type of gear in planetary gearboxes for both local and distributed damage cases. We can detect and locate planetary gearbox faults by monitoring the presence or amplitude changes of the sidebands associated with specific gear characteristic frequency in the spectral domain. Our work addresses the key issue from the root (such as: how is the spectral structure in terms of frequency components and their magnitudes, how to calculate the characteristic frequency of each type of gear in a planetary gearbox, and which frequency components to focus for fault diagnosis), and provides a theoretical guide for fault diagnosis of planetary gearboxes via spectral analysis.

In this paper, we firstly model the vibration signals of planetary gearboxes with gear damage, considering the AMFM effects induced by gear damage and time variant working condition, as well as the effect of vibration transfer paths, and derive the corresponding Fourier transform in closed form in Section 2. Then we give explicit equations to calculate the characteristic frequency of each gear fault for both local and distributed damage cases in Section 3. We validate the signal model using both a simulated signal and an industrial one, and further demonstrate the effectiveness of the theoretical analysis using the experimental datasets of manually created local pitting and naturally developed wear of a planetary gearbox in Sections 4 and 5. Finally, we draw conclusions in Section 6.

2. Planetary gearbox vibration signal model

In this section, we model the vibrations signals induced by either local or distributed gear damage using the same AMFM process. We do not differentiate the model between the local damage case and the distributed damage case,

because they all produce an AMFM effect to the gear meshing vibration, and the only difference lies in that the characteristic frequencies of the two gear fault cases are not the same. In the following, we model the damage induced vibration signal at the meshing location as an AMFM process firstly. Then we analyze the effect of vibration transfer paths on sensor perceived signals. Next, we focus on the sensor perceived signals with additional AM term due to time-varying transfer paths. Finally, we consider both the AM and FM effects caused by periodical changes in working conditions.

2.1. Signal model of damage induced vibration at meshing location

We first focus on the damage induced vibration signals at the meshing location when the damaged area goes into meshing, excluding the effect of transfer paths on vibration signals. In this case, the signal model is applicable to any gear system, either fixed shaft gears or planetary gear sets. Assume that a gear has local damage on the surface of a single tooth or distributed damage across every tooth. Such damage will produce sudden changes in the vibration signal as the damaged gear tooth meshes with the mating gear. These changes will not only modulate the amplitude but also the instantaneous frequency of vibration signals. Because the modulation is periodic with the characteristic frequency of damaged gear (for fixed shaft gears, it is the rotating frequency of damaged gear. Whereas for planetary gear sets, it is dependent on the gearbox configuration. In Section 3, we will give details on how to calculate the characteristic frequency of each gear in a planetary gearbox), the AM and FM functions may be represented by discrete Fourier series with the characteristic frequency of the damaged gear as the fundamental frequency. Under such assumptions, the vibration signal induced by gear damage at the meshing location can be modeled as an AMFM process, with the gear pair meshing frequency or its multiples as the signal carrier frequency, and the characteristic frequency of the damaged gear or its multiples as the modulating frequency [14–21]

$$x(t)=\sum_{k=0}^{K} a_k(t)\cos[2\pi k f_{\text{mesh}}t+b_k(t)+\theta_k], \tag{1}$$

where K is the highest order of AMFM to be considered, and

$$a_k(t)=c\sum_{n=0}^{N} A_{kn}\cos(2\pi n f_{\text{characteristic}}t+\phi_{kn})=c\left[1+\sum_{n=1}^{N} A_{kn}\cos(2\pi n f_{\text{characteristic}}t+\phi_{kn})\right], \tag{2}$$

$$b_k(t)=\sum_{l=1}^{L} B_{kl}\sin(2\pi l f_{\text{characteristic}}t+\varphi_{kl}), \tag{3}$$

are the AM and the FM functions respectively, $A_{kn}>0$ and $B_{kl}>0$ are the magnitude of AM and FM respectively, c is a dimensionless constant depending on signal amplitude (without losing generality, it is set to 1 for simplicity), f_{mesh} is the gear meshing frequency, $f_{\text{characteristic}}$ is the characteristic frequency of the faulty gear, θ, ϕ and φ are the initial phases of AM and FM respectively, and N and L are the highest order of AM and FM to be considered respectively. In Eq. (2), when $n=0$, $A_{k0}\equiv 1$ and $\phi_{k0}\equiv 0$.

Without loss of generality, we consider only the fundamental characteristic frequency of the damaged gear and the gear meshing frequency, then the vibration signal model of a faulty gear becomes

$$x(t)=\underbrace{[1+A\cos(2\pi f_{\text{characteristic}}t+\phi)]}_{\text{AM by faulty gear rotation}}\cos[2\pi f_{\text{mesh}}t+\underbrace{B\sin(2\pi f_{\text{characteristic}}t+\varphi)}_{\text{FM by faulty gear rotation}}+\theta]. \tag{4}$$

According to the identity

$$\exp(jz\sin\theta)=\sum_{m=-\infty}^{\infty} J_m(z)\exp(jm\theta) \tag{5}$$

where $J_m(z)$ is the Bessel function of the first kind with integer order m and argument z, Eq. (4) can be expanded as a sum of infinite harmonics [22]

$$x(t)=[1+A\cos(2\pi f_{\text{characteristic}}t+\phi)]\sum_{m=-\infty}^{\infty} J_m(B)\cos[2\pi(f_{\text{mesh}}+mf_{\text{characteristic}})t+m\varphi+\theta]. \tag{6}$$

Furthermore, according to the identities of trigonometric functions, Eq. (6) can be rewritten as

$$x(t)=h(f_{\text{characteristic}},0,0)+\frac{A}{2}\left[h(f_{\text{characteristic}}f_{\text{characteristic}},\phi)+h(f_{\text{characteristic}},-f_{\text{characteristic}},-\phi)\right], \tag{7}$$

where the intermediate function

$$h(f_{\text{characteristic}}f',\phi)=\sum_{m=-\infty}^{\infty} J_m(B)\cos\{2\pi[f_{\text{mesh}}+mf_{\text{characteristic}}+f']t+m\varphi+\theta+\phi\}. \tag{8}$$

Then, the Fourier transform of Eq. (7) can be deduced as

$$X(f) = H(f_{\text{characteristic}},0,0) + \frac{A}{2}\left[H(f_{\text{characteristic}},f_{\text{characteristic}},\phi) + H(f_{\text{characteristic}},-f_{\text{characteristic}},-\phi)\right], \tag{9}$$

where the intermediate function

$$H(f_{\text{characteristic}},f',\phi) = \sum_{m=-\infty}^{\infty} J_m(B)\delta\{f-[f_{\text{mesh}}+mf_{\text{characteristic}}+f']\}\exp[j(m\varphi+\theta+\phi)]. \tag{10}$$

From Eq. (9), we can observe the following. Without considering the transfer path effect, the damage induced vibration signal at the meshing location has sidebands around the meshing frequency f_{mesh}, with a sideband spacing equal to the characteristic frequency of the faulty gear $f_{\text{characteristic}}$.

For both the fixed shaft gears and the planetary gear set, the damage induced vibration signals at the meshing location have the same form. But the characteristic frequencies of the faulty gears in a planetary gearbox are different from the fixed shaft ones, even they run at an identical speed.

Moreover, the signal model in this section is adequate to describe the damage induced signal of fixed shaft gear systems, because the meshing location of fixed shaft gears is fixed with respect to the vibration sensor mounted on the gearbox casing. However, for planetary gear systems, this signal model is not adequate to characterize the gear damage induced vibration. We have to consider the effect of vibration transfer paths, because the meshing location of sun–planet or planet–ring gear pairs are time-varying, with respect to the fixed sensor.

2.2. Effect of transfer path on vibration signal

In most cases, the ring gear of a planetary gearbox is stationary, and sensors are mounted on the gearbox casing which is connected to or fastened to the ring gear directly. We consider only this case in this paper.

The damage induced vibration signal at the meshing location has three possible paths to go from its origin to the senor through solid mechanical components and their contacts, as shown in Fig. 1. Suppose the damage occurs on a planet gear. Through the first path, the damage induced vibration signal propagates from its origin to the ring gear firstly, then from the ring gear to the gearbox casing, and finally to the sensor. Whereas through the second path, the vibration signal follows a longer path, from its origin to the sun gear firstly, then from the sun gear to the shaft connected to the sun gear, next from the sun gear shaft to the supporting bearing, further from the bearing to the gearbox casing, and finally reaches the sensor. The third path is similar to the second one: the vibration signal goes from its origin to the planet gear carrier through the bearing and shaft supporting the planet gear firstly, then from the planet carrier to the planet carrier shaft, next from the planet carrier shaft to the bearing supporting the planet carrier shaft, further from the bearing to the gearbox casing and finally reaches the sensor.

If all the gears in the planetary gearbox are isotropic circumferentially, then the properties of the second and the third transfer paths do not change along time even though all the gears (except the ring gear) are rotating. The propagating distance for the damage induced signal goes from its origin to the sensor remains the same when the planet carrier and sun gear rotate, thus the transfer paths only make a scaling effect rather than an AM effect during the propagation of the damage induced vibration signal. Without loss of generality, the sensor perceived signal from the second and the third paths can be simplified as Eq. (4), and it has the same spectral structure as revealed by Eq. (9): the sensor perceived signal due to gear damage and from transfer paths 2 and 3 has sidebands around the meshing frequency f_{mesh}, with a sideband spacing equal to the characteristic frequency of faulty gear $f_{\text{characteristic}}$.

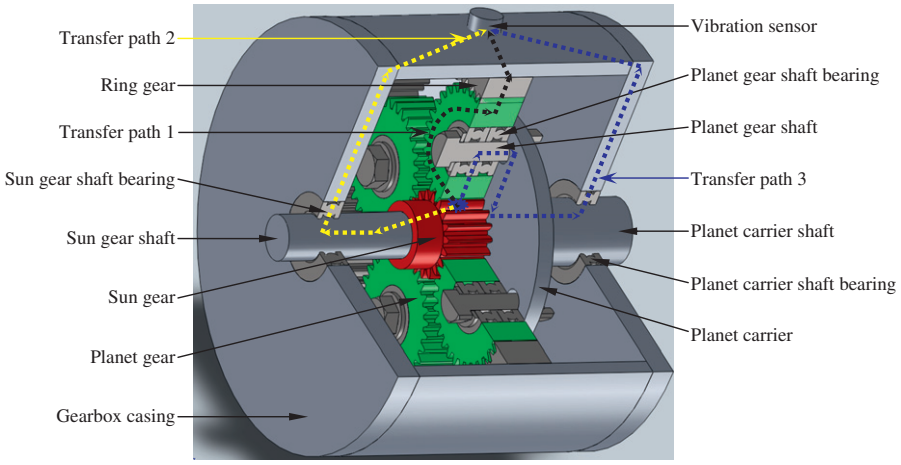

Fig. 1. Three transfer paths.

However, during the propagation through the second and the third paths, the damage induced vibration signal will be damped much by the longer transfer path, especially by the damping of bearings due to the complicated transfer path inside, and the sensor perceived signal will be most likely to have negligible amplitude. Hence, we do not further consider the cases of the second and third transfer paths.

On the other hand, the first path is shorter, compared with the second and the third transfer paths. It does not involve bearings which cause complicated attenuation on the signal, so the sensor perceived signal from the first path will contain much more information of the faulty gear. However, the transfer path for the damage induced signal going through the first path is time-varying except the case of ring gear damage, because the signal propagating distance is time-varying when the planet carrier and sun gear rotate. Regarding this issue, we will give sensor perceived signal model based on Eq. (4) for the cases of damage on each type of gears in the following sections.

Meanwhile, lubricating oil inside of planetary gearboxes may also transmit a little bit of gear vibration. However, the time variation of the transfer path through oil is similar to that of the first path through solid mechanical components and their contacts. For the ring gear damage case, whether the damage location is in the oil or not, the transfer path for the ring gear damage induced vibration to reach the sensor through oil is fixed. Then the transfer path through oil only has a scaling effect on the ring gear damage induced vibration signal. For the planet gear or the sun gear damage case, the transfer path for the gear damage induced vibration to reach the sensor through oil also changes periodically with the rotating planet carrier or the sun gear. Thus the AM effect of the time-varying transfer path through oil can be described using the same form of function as that of the first path through solid mechanical components and their contacts (to be considered in Sections 2.4 and 2.5). Moreover, during the propagation through oil, the gear damage induced vibration signal will be damped much by the damping of the lubricating oil, and the sensor perceived signal will be most likely to lose most energy of the vibration transmitted through oil. Hence, we do not consider in detail the effect of transfer path through oil, for two reasons: (1) it has a similar effect as the first path through solid mechanical components and their contacts, and thus its effect will be inherently included in the following discussion on the first path in Sections 2.3–2.5 and (2) the gear damage induced vibration signal through oil is negligible due to the damping of oil.

2.3. Sensor perceived signal model of damaged ring gear vibration

Suppose damage occurs on the ring gear. Since the vibration sensor is mounted on the gearbox casing and its position is fixed relative to any damaged ring gear tooth, the transfer path for the damage induced vibration signal propagating from the damaged ring gear tooth to the sensor does not vary even though the planet carrier rotates. Hence, the planet carrier rotation does not cause AM effect on the damage induced vibration during its propagation. The sensor perceived vibration signal due to ring gear damage has the same form as Eq. (4), and can be simplified as

$$x(t)=\underbrace{[1+A\cos(2\pi f_{\text{ring}}t+\phi)]}_{\text{AM by relative rotation of ring}}\cos[2\pi f_{\text{mesh}}t+\underbrace{B\sin(2\pi f_{\text{ring}}t+\varphi)}_{\text{FM by relative rotation of ring}}+\theta], \tag{11}$$

where f_{ring} is the characteristic frequency of faulty ring gear. How to calculate f_{ring} for local and distributed damage cases will be introduced in Section 3.3.

Similar to the procedure from Eqs. (4) through (10), the Fourier transform of Eq. (11) can be deduced as

$$X(f)=H(f_{\text{ring}},0,0)+\frac{A}{2}\left[H(f_{\text{ring}},f_{\text{ring}},\phi)+H(f_{\text{ring}},-f_{\text{ring}},-\phi)\right]. \tag{12}$$

From Eq. (12), we can observe the following. For a faulty planetary gearbox with a damaged ring gear, the vibration signal has sidebands around the meshing frequency f_{mesh}, with a sideband spacing equal to the characteristic frequency of the faulty ring gear f_{ring}.

For the cases that the signal travel through the second and the third transfer paths, since the transfer paths have a scaling effect during the propagation of the damage induced vibration signal, the sensor perceived signals have the same form as Eqs. (4) and (11), and their spectral structure are also the same as Eq. (12).

If we consider the AMFM effects with the higher orders of faulty ring gear characteristic frequency nf_{ring} as the modulating frequency and with the higher orders of meshing frequency kf_{mesh} as the signal carrier frequency, peaks will appear at the frequency locations of $kf_{\text{mesh}}\pm nf_{\text{ring}}$ in the Fourier spectrum. Since the spectral peaks of the ring gear damage induced vibration signal are associated with the characteristic frequency of the faulty ring gear, we expect to detect and locate the ring gear fault by monitoring the presence or magnitude increase of spectral peaks at the frequency locations of $kf_{\text{mesh}}\pm nf_{\text{ring}}$, $k,n=1,2,\ldots$.

2.4. Sensor perceived signal model of damaged planet gear vibration

When damage occurs on a planet gear, the meshing location of the damaged area with the mating gear (either ring gear or sun gear) relative to the fixed sensor will change with the planet carrier rotation. Thus the relative motion of the meshing location will cause the change of transfer path for the damage induced vibration propagating from the meshing location to the sensor, and thereby will produce an AM effect on the vibration signal during its propagation. Suppose the

damaged planet gear starts meshing at the location farthest from (i.e. opposite to) the sensor. When the planet gear approaches to the sensor, the measured vibration due to damage will increase, reaching its maximum when the damaged planet gear goes into meshing at a location closest to the sensor. When the planet gear goes away from the sensor, the measured vibration caused by the damage will decrease, diminishing to its minimum when the damaged planet gear goes into meshing at a location farthest from (opposite to) the sensor. This AM effect can be modeled by a Hanning function [12,13]. Hence, an additional multiplicative term due to the planet carrier rotation induced AM effect is added to Eq. (4), and the sensor perceived signal due to planet gear damage can be modeled as

$$x(t)=\underbrace{[1-\cos(2\pi f_{\text{carrier}}t)]}_{\text{AMbycarrierrotation}}\underbrace{[1+A\cos(2\pi f_{\text{planet}}t+\phi)]}_{\text{AM by relative rotation of planet}}\cos[2\pi f_{\text{mesh}}t+\underbrace{B\sin(2\pi f_{\text{planet}}t+\varphi)}_{\text{FM by relative rotation of planet}}+\theta], \tag{13}$$

where f_{carrier} is the rotating frequency of planet carrier and f_{planet} is the characteristic frequency of faulty planet gear. How to calculate f_{planet} for local and distributed damage cases will be introduced in Section 3.1.

Following the same procedure as detailed in Section 2.1, Eq. (13) can be expanded as

$$\begin{aligned}x(t)=&\,h(f_{\text{planet}},0,0)+\frac{A}{2}\left[h(f_{\text{planet}},f_{\text{planet}},\phi)+h(f_{\text{planet}},-f_{\text{planet}},-\phi)\right]-\frac{1}{2}\left[h(f_{\text{planet}},f_{\text{carrier}},0)+h(f_{\text{planet}},-f_{\text{carrier}},0)\right]\\&-\frac{A}{4}\left[h(f_{\text{planet}},f_{\text{planet}}+f_{\text{carrier}},\phi)+h(f_{\text{planet}},f_{\text{planet}}-f_{\text{carrier}},\phi)\right]-\frac{A}{4}\left[h(f_{\text{planet}},-f_{\text{planet}}+f_{\text{carrier}},-\phi)+h(f_{\text{planet}},-f_{\text{planet}}-f_{\text{carrier}},-\phi)\right].\end{aligned} \tag{14}$$

The Fourier transform of Eq. (14) can be derived as

$$\begin{aligned}X(f)=&\,H(f_{\text{planet}},0,0)+\frac{A}{2}\left[H(f_{\text{planet}},f_{\text{planet}},\phi)+H(f_{\text{planet}},-f_{\text{planet}},-\phi)\right]-\frac{1}{2}\left[H(f_{\text{planet}},f_{\text{carrier}},0)+H(f_{\text{planet}},-f_{\text{carrier}},0)\right]\\&-\frac{A}{4}\left[H(f_{\text{planet}},f_{\text{planet}}+f_{\text{carrier}},\phi)+H(f_{\text{planet}},f_{\text{planet}}-f_{\text{carrier}},\phi)\right]-\frac{A}{4}\left[H(f_{\text{planet}},-f_{\text{planet}}+f_{\text{carrier}},-\phi)\right.\\&\left.+H(f_{\text{planet}},-f_{\text{planet}}-f_{\text{carrier}},-\phi)\right].\end{aligned} \tag{15}$$

From Eq. (15), we can observe the following. For a planetary gearbox with a damaged planet gear, the sensor perceived vibration signal has sidebands around three centers which are the meshing frequency f_{mesh}, and the meshing frequency minus and plus the planet carrier rotating frequency $f_{\text{mesh}}\pm f_{\text{carrier}}$, with a sideband spacing equal to the characteristic frequency of faulty planet gear f_{planet}.

For the cases that the signal travel through the second and the third transfer paths, since the transfer paths have a scaling effect during the propagation of the damage induced vibration signal, the sensor perceived signals have the same form as Eq. (4), and their spectral structure are also the same as Eq. (9). Sidebands appear around the meshing frequency f_{mesh}, with a sideband spacing equal to the characteristic frequency of faulty planet gear f_{planet}.

If we consider the AMFM effects with the higher orders of faulty planet gear characteristic frequency nf_{planet} as the modulating frequency and with the higher orders of meshing frequency kf_{mesh} as the signal carrier frequency, peaks will appear at the frequency locations of $kf_{\text{mesh}}\pm nf_{\text{planet}}$ and $kf_{\text{mesh}}\pm f_{\text{carrier}}\pm nf_{\text{planet}}$ in the Fourier spectrum. Since the spectral peaks of planet gear damage induced vibration signal are associated with the characteristic frequency of faulty planet gear, we can detect and locate the planet gear fault by monitoring the presence or magnitude increase of spectral peaks at the frequency locations of $kf_{\text{mesh}}\pm nf_{\text{planet}}$ and $kf_{\text{mesh}}\pm f_{\text{carrier}}\pm nf_{\text{planet}}$, $k,n=1,2,\ldots$.

2.5. Sensor perceived signal model of damaged sun gear vibration

When damage occurs on the sun gear, the meshing location of the damaged area with any mating planet gear will also change with the sun gear rotation. This will produce an AM effect on the damage induced vibration during its propagation too. Similarly, an additional multiplicative term due to the sun gear rotation induced AM effect is added to Eq. (4), and the sensor perceived signal due to sun gear damage can be modeled as

$$x(t)=\underbrace{[1-\cos(2\pi f_{\text{sunrot}}t)]}_{\text{AM by sun rotation}}\underbrace{[1+A\cos(2\pi f_{\text{sun}}t+\phi)]}_{\text{AM by relative rotation of sun}}\cos[2\pi f_{\text{mesh}}t+\underbrace{B\sin(2\pi f_{\text{sun}}t+\varphi)}_{\text{FM by relative rotation of sun}}+\theta]. \tag{16}$$

where f_{sunrot} is the rotating frequency of the sun gear and f_{sun} is the characteristic frequency of faulty sun gear. How to calculate f_{sun} for local and distributed damage cases will be introduced in Section 3.2.

Following the same procedure as detailed in Section 2.1, Eq. (16) can be expanded as

$$\begin{aligned}x(t)=&\,h(f_{\text{sun}},0,0)+\frac{A}{2}\left[h(f_{\text{sun}},f_{\text{sun}},\phi)+h(f_{\text{sun}},-f_{\text{sun}},-\phi)\right],-\frac{1}{2}\left[h(f_{\text{sun}},f_{\text{sunrot}},0)+h(f_{\text{sun}},-f_{\text{sunrot}},0)\right]\\&-\frac{A}{4}\left[h(f_{\text{sun}},f_{\text{sun}}+f_{\text{sunrot}},\phi)+h(f_{\text{sun}},f_{\text{sun}}-f_{\text{sunrot}},\phi)\right]-\frac{A}{4}\left[h(f_{\text{sun}},-f_{\text{sun}}+f_{\text{sunrot}},-\phi)+h(f_{\text{sun}},-f_{\text{sun}}-f_{\text{sunrot}},-\phi)\right]\end{aligned} \tag{17}$$

The Fourier transform of Eq. (17) can be derived as

$$x(t)=H(f_{\text{sun}},0,0)+\frac{A}{2}\left[H(f_{\text{sun}},f_{\text{sun}},\phi)+H(f_{\text{sun}},-f_{\text{sun}},-\phi)\right]-\frac{1}{2}\left[H(f_{\text{sun}},f_{\text{sunrot}},0)+H(f_{\text{sun}},-f_{\text{sunrot}},0)\right]$$
$$-\frac{A}{4}\left[H(f_{\text{sun}},f_{\text{sun}}+f_{\text{sunrot}},\phi)+H(f_{\text{sun}},f_{\text{sun}}-f_{\text{sunrot}},\phi)\right]-\frac{A}{4}\left[H(f_{\text{sun}},-f_{\text{sun}}+f_{\text{sunrot}},-\phi)+H(f_{\text{sun}},-f_{\text{sun}}-f_{\text{sunrot}},-\phi)\right]. \quad (18)$$

From Eq. (18), we can observe the following. For a planetary gearbox with a damaged sun gear, the sensor perceived vibration signal has sidebands around three centers which are the meshing frequency f_{mesh} and the meshing frequency minus and plus the rotating frequency of sun gear $f_{\text{mesh}}\pm f_{\text{sunrot}}$, with a sideband spacing equal to the characteristic frequency of faulty sun gear f_{sun}.

For the cases that the signal travel through the second and third transfer paths, since the transfer paths have a scaling effect during the propagation of the damage induced vibration signal, the sensor perceived signals have the same form as Eq. (4), and their spectral structure are also the same as Eq. (9). Sidebands appear around the meshing frequency f_{mesh}, with a sideband spacing equal to the characteristic frequency of faulty sun gear f_{sun}.

If we consider the AMFM effects with the higher orders of faulty sun gear characteristic frequency nf_{sun} as the modulating frequency and with the higher orders of meshing frequency kf_{mesh} as the signal carrier frequency, peaks will appear at the frequency locations of $kf_{\text{mesh}}\pm nf_{\text{sun}}$ and $kf_{\text{mesh}}\pm f_{\text{sunrot}}\pm nf_{\text{sun}}$ in the Fourier spectrum. Since the spectral peaks of sun gear damage induced vibration signal are associated with the characteristic frequency of faulty sun gear, we can detect and locate the sun gear fault by monitoring the presence or magnitude increase of spectral peaks at the frequency locations of $kf_{\text{mesh}}\pm nf_{\text{sun}}$ and $kf_{\text{mesh}}\pm f_{\text{sunrot}}\pm nf_{\text{sun}}$, $k,n=1,2,\ldots$.

2.6. Sensor perceived signal model under periodically varying condition

In above theoretical analysis, the working condition of planetary gearboxes is assumed to be constant. However, in some cases, the running speed or load may change periodically [8], thus produce additional AM and FM effects on the gear damage induced vibration signal. Under such periodically variant conditions, the sensor perceived signal model, Eqs. (11), (13) and (16), can be modified into a general model

$$x(t)=\underbrace{[1-\cos(2\pi f_{\text{rotating}}t)]}_{\text{AM by variation in transfer path}}\ \underbrace{[1+A_{\text{condition}}\cos(2\pi f_{\text{condition}}t+\varphi)]}_{\text{AM by variation in condition}}\underbrace{[1+A_{\text{fault}}\cos(2\pi f_{\text{characteristic}}t+\phi)]}_{\text{AM by faulty gear rotation}}$$
$$\times\cos[2\pi f_{\text{mesh}}t+\underbrace{B_{\text{fault}}\sin(2\pi f_{\text{characteristic}}t+\alpha)}_{\text{FM by faulty gear rotation}}+\underbrace{B_{\text{condition}}\sin(2\pi f_{\text{condition}}t+\beta)}_{\text{FM by variation incondition}}+\theta], \quad (19)$$

where $A_{\text{condition}}$ and $B_{\text{condition}}$ are the AM and FM magnitudes caused by periodical variation in working conditions, A_{fault} and B_{fault} are the AM and FM magnitudes produced by gear damage, f_{rotating} is the rotating frequency of the planet carrier or sun gear (Note: In this section, we only consider the complicated cases of planet or sun gear damage. For ring gear damage case, we can easily derive similar results by omitting the cosine term containing f_{rotating} because the transfer path is fixed), $f_{\text{condition}}$ is the varying frequency of working condition, $f_{\text{characteristic}}$ is the characteristic frequency of faulty gear, and α, β, ϕ, φ and θ are initial phases.

According to the properties of Bessel functions and the identities of trigonometric functions, Eq. (19) can be rewritten as

$$x(t)=h'(0,0)-\frac{1}{2}\left[h'(f_{\text{rotating}},0)+h'(-f_{\text{rotating}},0)\right]+\frac{1}{2}A_{\text{condition}}\left[h'(f_{\text{condition}},\varphi)+h'(-f_{\text{condition}},-\varphi)\right]$$
$$+\frac{1}{2}A_{\text{fault}}\left[h'(f_{\text{characteristic}},\phi)+h'(-f_{\text{characteristic}},-\phi)\right]-\frac{1}{4}A_{\text{condition}}\left[h'(f_{\text{rotating}}+f_{\text{condition}},\varphi)+h'(-f_{\text{rotating}}-f_{\text{condition}},-\varphi)\right.$$
$$\left.+h'(-f_{\text{rotating}}+f_{\text{condition}},\varphi)+h'(f_{\text{rotating}}-f_{\text{condition}},-\varphi)\right]-\frac{1}{4}A_{\text{fault}}\left[h'(f_{\text{rotating}}+f_{\text{characteristic}},\phi)+h'(-f_{\text{rotating}}-f_{\text{characteristic}},-\phi)\right.$$
$$\left.+h'(-f_{\text{rotating}}+f_{\text{characteristic}},\phi)+h'(f_{\text{rotating}}-f_{\text{characteristic}},-\phi)\right]+\frac{1}{4}A_{\text{fault}}A_{\text{condition}}\left[h'(f_{\text{condition}}+f_{\text{characteristic}},\varphi+\phi)\right.$$
$$\left.+h'(-f_{\text{condition}}-f_{\text{characteristic}},-\varphi-\phi)+h'(-f_{\text{condition}}+f_{\text{characteristic}},-\varphi+\phi)+h'(f_{\text{condition}}-f_{\text{characteristic}},\varphi-\phi)\right]$$
$$-\frac{1}{8}A_{\text{condition}}A_{\text{fault}}\left[h'(f_{\text{rotating}}+f_{\text{condition}}+f_{\text{characteristic}},\varphi+\phi)+h'(-f_{\text{rotating}}-f_{\text{condition}}-f_{\text{characteristic}},-\varphi-\phi)\right.$$
$$+h'(f_{\text{rotating}}+f_{\text{condition}}-f_{\text{characteristic}},\varphi-\phi)+h'(-f_{\text{rotating}}-f_{\text{condition}}+f_{\text{characteristic}},-\varphi+\phi)+h'(-f_{\text{rotating}}+f_{\text{condition}}$$
$$+f_{\text{characteristic}},\varphi+\phi)+h'(f_{\text{rotating}}-f_{\text{condition}}-f_{\text{characteristic}},-\varphi-\phi)+h'(-f_{\text{rotating}}+f_{\text{condition}}-f_{\text{characteristic}},\varphi-\phi)$$
$$\left.+h'(f_{\text{rotating}}-f_{\text{condition}}+f_{\text{characteristic}},-\varphi+\phi)\right], \quad (20)$$

where the intermediate function

$$h'(f',\varphi)=\sum_{m'=-\infty}^{\infty}J_{m'}(B_{\text{condition}})\sum_{m=-\infty}^{\infty}J_m(B_{\text{fault}})\cos\{2\pi[f_{\text{mesh}}+mf_{\text{characteristic}}+m'f_{\text{condition}}+f']t+m\alpha+m'\beta+\theta+\varphi\}. \quad (21)$$

Furthermore, the Fourier transform of Eq. (20) can be deduced as

$$\begin{aligned}X(f)=H'(0,0)&-\frac{1}{2}\left[H'(f_{\text{rotating}},0)+H'(-f_{\text{rotating}},0)\right]+\frac{1}{2}A_{\text{condition}}\left[H'(f_{\text{condition}},\varphi)+H'(-f_{\text{condition}},-\varphi)\right]+\frac{1}{2}A_{\text{fault}}\left[H'(f_{\text{characteristic}},\phi)\right.\\&\left.+H'(-f_{\text{characteristic}},-\phi)\right]-\frac{1}{4}A_{\text{condition}}\left[H'(f_{\text{rotating}}+f_{\text{condition}},\varphi)+H'(-f_{\text{rotating}}-f_{\text{condition}},-\varphi)+H'(-f_{\text{rotating}}+f_{\text{condition}},\varphi)\right.\\&\left.+H'(f_{\text{rotating}}-f_{\text{condition}},-\varphi)\right]-\frac{1}{4}A_{\text{fault}}\left[H'(f_{\text{rotating}}+f_{\text{characteristic}},\phi)+H'(-f_{\text{rotating}}-f_{\text{characteristic}},-\phi)\right.\\&\left.+H'(-f_{\text{rotating}}+f_{\text{characteristic}},\phi)+H'(f_{\text{rotating}}-f_{\text{characteristic}},-\phi)\right]+\frac{1}{4}A_{\text{fault}}A_{\text{condition}}\left[H'(f_{\text{condition}}+f_{\text{characteristic}},\varphi+\phi)\right.\\&\left.+H'(-f_{\text{condition}}-f_{\text{characteristic}},-\varphi-\phi)+H'(-f_{\text{condition}}+f_{\text{characteristic}},-\varphi+\phi)+H'(f_{\text{condition}}-f_{\text{characteristic}},\varphi-\phi)\right]\\&-\frac{1}{8}A_{\text{condition}}A_{\text{fault}}\left[H'(f_{\text{rotating}}+f_{\text{condition}}+f_{\text{characteristic}},\varphi+\phi)+H'(-f_{\text{rotating}}-f_{\text{condition}}-f_{\text{characteristic}},-\varphi-\phi)\right.\\&+H'(f_{\text{rotating}}+f_{\text{condition}}-f_{\text{characteristic}},\varphi-\phi)+H'(-f_{\text{rotating}}-f_{\text{condition}}+f_{\text{characteristic}},-\varphi+\phi)\\&+H'(-f_{\text{rotating}}+f_{\text{condition}}+f_{\text{characteristic}},\varphi+\phi)+H'(f_{\text{rotating}}-f_{\text{condition}}-f_{\text{characteristic}},-\varphi-\phi)\\&\left.+H'(-f_{\text{rotating}}+f_{\text{condition}}-f_{\text{characteristic}},\varphi-\phi)+H'(f_{\text{rotating}}-f_{\text{condition}}+f_{\text{characteristic}},-\varphi+\phi)\right],\end{aligned}\tag{22}$$

where the intermediate function

$$H'(f',\varphi)=\sum_{m'=-\infty}^{\infty}J_{m'}(B_{\text{condition}})\sum_{m=-\infty}^{\infty}J_m(B_{\text{fault}})\delta\{f-[f_{\text{mesh}}+mf_{\text{characteristic}}+m'f_{\text{condition}}+f']\}\times\exp[j(m\alpha+m'\beta+\theta+\varphi)].\tag{23}$$

From Eq. (22), we can observe the following. For a faulty planetary gearbox with a damaged planet or sun gear and under periodically variant working condition, the sensor perceived vibration signal has sidebands around the meshing frequency f_{mesh}, and the meshing frequency minus and plus the rotating frequency of planet carrier or sun gear $f_{\text{mesh}}\pm f_{\text{rotating}}$, with a sideband spacing equal to the characteristic frequency of faulty gear $f_{\text{characteristic}}$, the varying frequency of working condition $f_{\text{condition}}$, or their combinations $f_{\text{characteristic}}\pm f_{\text{condition}}$.

For the cases that the signal travel through the second and third transfer paths, sidebands appear around the meshing frequency f_{mesh}, with a sideband spacing equal to the characteristic frequency of faulty gear $f_{\text{characteristic}}$, the varying frequency of working condition $f_{\text{condition}}$, or their combinations $f_{\text{characteristic}}\pm f_{\text{condition}}$.

If we consider the AMFM effects with the higher orders of faulty gear characteristic frequency $mf_{\text{characteristic}}$ and the higher orders of working condition varying frequency $m'f_{\text{condition}}$ as the modulating frequency and with the higher orders of meshing frequency kf_{mesh} as the signal carrier frequency, peaks will appear at the frequency locations of $kf_{\text{mesh}}\pm mf_{\text{characteristic}}\pm m'f_{\text{condition}}$ and $kf_{\text{mesh}}\pm f_{\text{rotating}}\pm mf_{\text{characteristic}}\pm m'f_{\text{condition}}$ $(k,m,m'=0,1,2,\ldots)$ in the Fourier spectrum.

Though the spectral structure of the modified signal model is more complicated, we can still detect and locate the gear damage by monitoring the presence or magnitude change of the sidebands at the frequency locations of $kf_{\text{mesh}}\pm mf_{\text{characteristic}}$ and $kf_{\text{mesh}}\pm f_{\text{rotating}}\pm mf_{\text{characteristic}}$, because these sidebands are closely related to the gear damage. For example, we investigate the sidebands at the frequency locations of $f_{\text{mesh}}\pm mf_{\text{characteristic}}$. From Eq. (22), we can see that these sidebands form a regular group around the meshing frequency f_{mesh} with a spacing of $f_{\text{characteristic}}$, which are caused by and correspond to the gear damage. The spectral amplitude at the frequency locations of $f_{\text{mesh}}\pm mf_{\text{characteristic}}$ can be derived from Eq. (22)

$$\begin{aligned}X(f_{\text{mesh}}\pm mf_{\text{characteristic}})&=J_0(B_{\text{condition}})J_{\pm m}(B_{\text{fault}})\exp\left[j(\pm m\alpha+\theta)\right]\\&+\frac{1}{2}A_{\text{fault}}J_0(B_{\text{condition}})J_{\pm m-1}(B_{\text{fault}})\exp\{j\left[(\pm m-1)\alpha+\theta+\phi)\right]\}\\&+\frac{1}{2}A_{\text{fault}}J_0(B_{\text{condition}})J_{\pm m+1}(B_{\text{fault}})\exp\{j\left[(\pm m+1)\alpha+\theta-\phi)\right]\}\\&+\frac{1}{2}A_{\text{condition}}J_{-1}(B_{\text{condition}})J_{\pm m}(B_{\text{fault}})\exp\left[j(\pm m\alpha-\beta+\theta+\varphi)\right]\\&+\frac{1}{2}A_{\text{condition}}J_1(B_{\text{condition}})J_{\pm m}(B_{\text{fault}})\exp\left[j(\pm m\alpha+\beta+\theta-\varphi)\right]\\&+\frac{1}{4}A_{\text{fault}}A_{\text{condition}}J_{-1}(B_{\text{condition}})J_{\pm m-1}(B_{\text{fault}})\exp\{j\left[(\pm m-1)\alpha-\beta+\theta+\phi+\varphi)\right]\}\\&+\frac{1}{4}A_{\text{fault}}A_{\text{condition}}J_1(B_{\text{condition}})J_{\pm m+1}(B_{\text{fault}})\exp\{j\left[(\pm m+1)\alpha+\beta+\theta-\phi-\varphi)\right]\}\\&+\frac{1}{4}A_{\text{fault}}A_{\text{condition}}J_1(B_{\text{condition}})J_{\pm m-1}(B_{\text{fault}})\exp\{j\left[(\pm m-1)\alpha+\beta+\theta+\phi-\varphi)\right]\}\\&+\frac{1}{4}A_{\text{fault}}A_{\text{condition}}J_{-1}(B_{\text{condition}})J_{\pm m+1}(B_{\text{fault}})\exp\{j\left[(\pm m+1)\alpha-\beta+\theta-\phi+\varphi)\right]\}.\end{aligned}\tag{24}$$

Since the variations in working condition are supposed to be periodical, the varying frequency $f_{\text{condition}}$, the AM and FM magnitudes $A_{\text{condition}}$ and $B_{\text{condition}}$, and the associated phases ϕ and β are constant. Then from Eq. (24), we can see that the sideband amplitude are only dependent on the AM and FM magnitudes A_{fault} and B_{fault} associated with gear damage, and the sideband order m. Therefore, we can still detect and locate the gear fault by the presence or magnitude change of sidebands at the frequency of $f_{\text{mesh}}\pm mf_{\text{characteristic}}$.

We should note here that if the AMFM effect by periodically variant working condition is assumed to be produced by damage on another type of gear, then the theoretical derivations in this section, Eqs. (19)–(24), can be generalized to diagnose compound damage on different type of gears in planetary gearboxes.

In most cases, planetary gearboxes run under constant conditions or periodically time variant conditions, thus the theoretical derivations in Sections 2.3–2.6 are applicable. Sometimes, transient changes in the working condition may occur without any period. In such cases, for fault diagnosis purpose, we can run planetary gearboxes at constant condition (idling, for example) for a while, thus enable the spectral analysis to be suitable to analyze the collected stationary signals. Moreover, in a short time, the working condition often does not change too much because of the inertia of planetary gearboxes and connected machinery. Thus, the signals in a proper short time window can be assumed to be stationary, and spectral analysis is still suitable to analyze such short time signals (Section 4.2 will show this).

Since the characteristic frequency of each gear, f_{ring}, f_{planet} and f_{sun}, is important for fault diagnosis of planetary gearboxes, we will introduce how to calculate these frequencies given the configuration and running speed of gearboxes in Section 3.

3. Characteristic frequency of faulty gear in planetary gearbox

For local damage case, the characteristic frequency of a faulty gear in planetary gearboxes is defined as how many times that the faulty gear tooth meshes with mating gears per unit time, because the local gear damage modulates gear meshing vibration at the repeating frequency of the sudden changes caused by the contact of the locally damaged gear tooth with mating gears. While for distributed damage case, it is defined as the relative rotating frequency of the faulty gear with respect to the planet carrier, because the distributed gear damage modulates gear meshing vibration at a period equal to the damaged gear rotating cycle relative to the planer carrier.

In a single stage planetary gearbox, the two types of gear pair, sun–planet and planet–ring, have an identical meshing frequency. In most cases, the ring gear is stationary, then the meshing frequency equals the product of planet carrier rotating frequency f_{carrier} and the number of ring gear teeth Z_{ring}

$$f_{\text{mesh}} = f_{\text{carrier}} Z_{\text{ring}}. \tag{25}$$

The meshing frequency of a gear of interest means how many gear teeth get involved in meshing per unit time. Given the meshing frequency of a single stage planetary gearbox f_{mesh} and the total number of teeth of a gear of interest Z, the quotient

$$f_{\text{relative}} = \frac{f_{\text{mesh}}}{Z}, \tag{26}$$

means how many revolutions that the gear of interest rotates per unit time, i.e. the relative rotating frequency with respect to the planet carrier.

3.1. Faulty planet gear

For local damage case, suppose a single damage occurs on a planet gear tooth surface. If the damage exists on one side of the gear tooth, in one relative rotating cycle with respect to the planet carrier, the damaged area on the planet gear will contact with one mating gear (either sun gear or ring gear) once, and a sudden change in vibration will be generated. So the characteristic frequency of faulty planet gear is

$$f_{\text{planet 1}} = \frac{f_{\text{mesh}}}{Z_{\text{planet}}}, \tag{27}$$

where Z_{planet} is the number of planet gear teeth.

If the damage exists on both sides of the gear tooth, the damaged planet gear tooth also meshes with the other mating gear, it might cause a sudden change in vibration too. In this case, the characteristic frequency of the faulty planet gear becomes twice of Eq. (27)

$$f_{\text{planet 2}} = 2\frac{f_{\text{mesh}}}{Z_{\text{planet}}}. \tag{28}$$

For distributed damage case, suppose damage occurs on every planet gear tooth. Then the distributed damage produce periodical changes as every damaged tooth gets in mesh, but the envelope amplitude of these periodical changes fluctuates at a frequency equal to the planet gear rotating frequency relative to the planet carrier. So the characteristic frequency of faulty planet gear becomes

$$f_{\text{planet}} = \frac{f_{\text{mesh}}}{Z_{\text{planet}}}. \tag{29}$$

3.2. Faulty sun gear

For local damage case, suppose a single damage occurs on a sun gear tooth surface. Each time the damaged area contacts with one of the mating planet gears, a sudden change in vibration will be generated. In one relative rotating cycle with respect to the planet carrier, the damaged area will contact with all the planet gears. So the characteristic frequency of the faulty sun gear equals the relative rotating frequency of the sun gear multiplied by the number of planet gears

$$f_{\text{sun}} = \frac{f_{\text{mesh}}}{Z_{\text{sun}}} N_{\text{planet}}, \tag{30}$$

where Z_{sun} is the number of sun gear teeth and N_{planet} is the number of planet gears.

For distributed damage case, similar to the derivation of Eq. (29), the characteristic frequency of faulty sun gear is

$$f_{\text{sun}} = \frac{f_{\text{mesh}}}{Z_{\text{sun}}}. \tag{31}$$

3.3. Faulty ring gear

For local damage case, similar to the derivation of Eq. (30), the characteristic frequency of faulty ring gear is

$$f_{\text{ring}} = \frac{f_{\text{mesh}}}{Z_{\text{ring}}} N_{\text{planet}}. \tag{32}$$

Similarly, for distributed damage case, the characteristic frequency of faulty ring gear is

$$f_{\text{ring}} = \frac{f_{\text{mesh}}}{Z_{\text{ring}}}. \tag{33}$$

Given the configuration parameters of a planetary gearbox, such as the number of teeth of each gear and the number of planet gears, as well as the gearbox running speed, the characteristic frequency of each faulty gear can be calculated according to Eqs. (27)–(33), for either local or distributed damage case. According to the theoretical analysis, by investigating the sideband structure and checking whether the sidebands location is associated with any of these characteristic frequencies, the gear fault can be detected and located.

4. Simulated and industrial signal analysis

4.1. Simulated signal analysis

To validate the above theoretical derivations and to illustrate the spectral structure of planetary gearbox vibration signals, we generate and analyze two signals simulating the vibration induced by local damage on a planet gear tooth: one is according to Eq. (4) which mimics the local damage induced vibration signals at meshing location excluding transfer path effect, and the other is according to Eq. (13) which includes the AM effect due to planet carrier rotation. The parameters used in the simulation are listed in Table 1. The signals are sampled at a frequency of 256 Hz.

Figs. 2 and 3 show the two simulated signals. For the first signal without considering the AM effect caused by planet carrier rotation, the spectral peaks appear as sidebands around the meshing frequency, at the frequencies of $f_{\text{mesh}} \pm kf_{\text{planet1}}$, $k = 1,2,\ldots$. This behavior is consistent with the expectation from Eq. (9).

For the second signal including the AM effect caused by planet carrier rotation, more spectral peaks appear as sidebands when we compare Fig. 3(b) with 2(b). These sidebands center around the meshing frequency and the meshing frequency plus and minus the planet carrier rotating frequency, at the frequencies of $f_{\text{mesh}} \pm kf_{\text{planet1}}$ and $f_{\text{mesh}} \pm f_{\text{carrier}} \pm kf_{\text{planet1}}$ (where $k = 1,2,\ldots$). This behavior is consistent with the expectation from Eq. (15).

4.2. Industrial signal analysis

To validate the applicability of the proposed AMFM model to describe industrial planetary gearbox vibration signals, we further analyze the collected vibration signal of a planetary gearbox in an oil sand industry. Fig. 4 shows the gearbox configuration, and Table 2 lists the gear parameter. An accelerometer was mounted on the casing of the 1st stage planetary gearbox. The vibration signals were collected during a normal industrial running of the gearbox at a sampling frequency of

Table 1
Parameters in simulation.

AM magnitude A	FM magnitude B	Meshing frequency (Hz)	Rotating frequency of planet carrier (Hz)	Characteristic frequency of faulty planet gear (Hz)
1	0.5	11.97	0.1478	0.3861

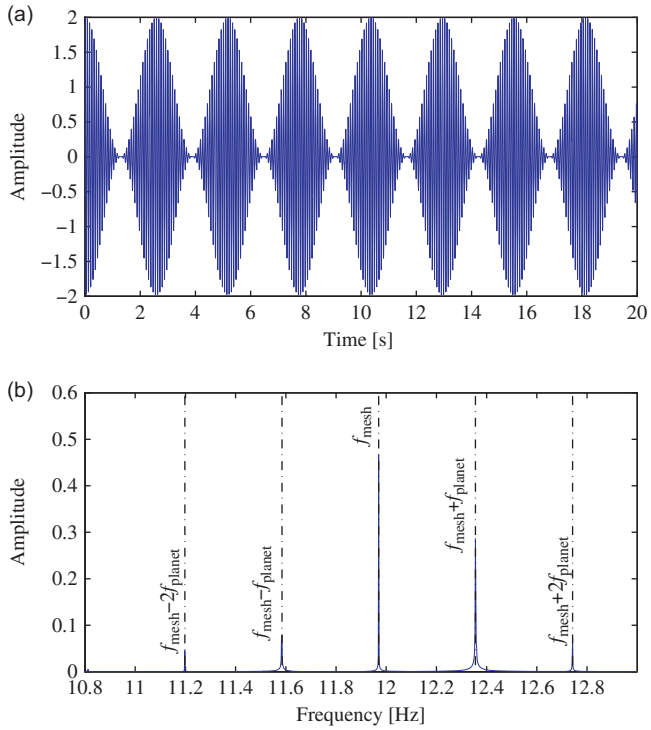

Fig. 2. Simulated planet gear damage induced signal excluding transfer path effect: (a) waveform and (b) Fourier spectrum.

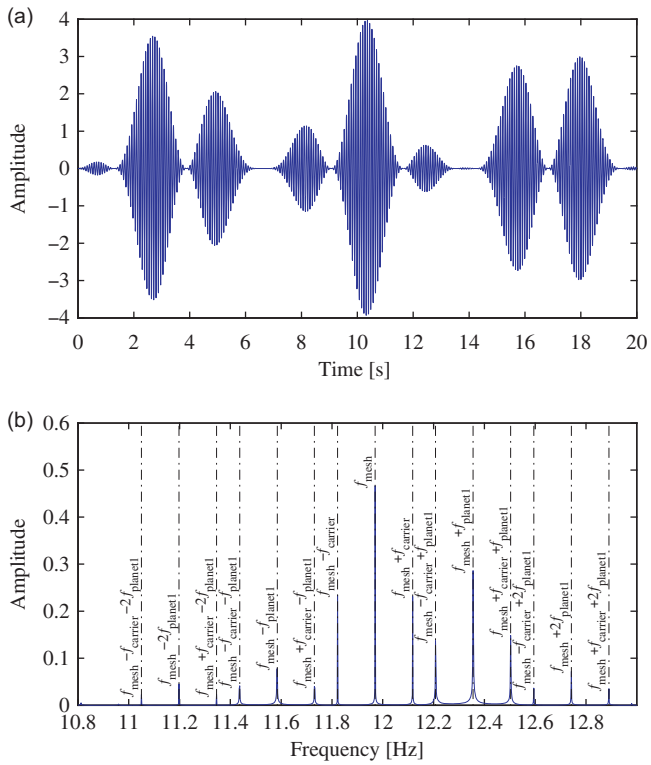

Fig. 3. Simulated planet gear damage induced signal including planet carrier rotation effect: (a) waveform and (b) Fourier spectrum.

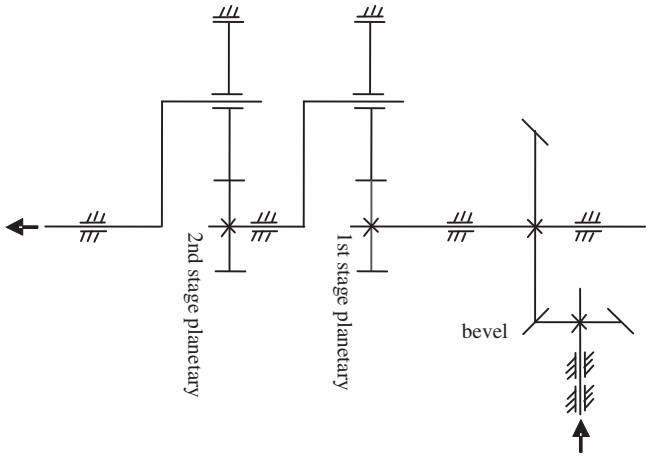

Fig. 4. Transmission diagram of industrial gearbox.

Table 2
Gear parameters of industrial gearbox.

Gearbox	Bevel		1st stage planetary			2nd stage planetary		
Gear	Input	Output	Sun	Planet	Ring	Sun	Planet	Ring
Number of teeth	11	49	28	62 (3)	152	19	31 (4)	81

Note: The number of planet gears is indicated in the parenthesis.

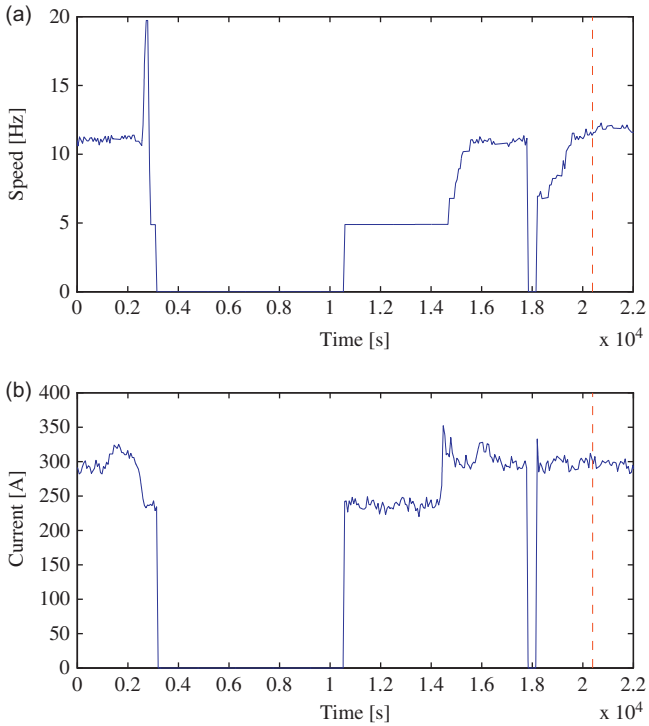

Fig. 5. Running conditions of driving motor: (a) speed and (b) current. (For interpretation of the references to color in this figure, the reader is referred to the web version of this article.)

4000 Hz, and 64,000 samples was recorded for each signal. Meanwhile, the running condition parameters, such as the speed and current of the driving motor connected to the bevel gearbox input shaft, were also recorded every second by an online monitoring and control system.

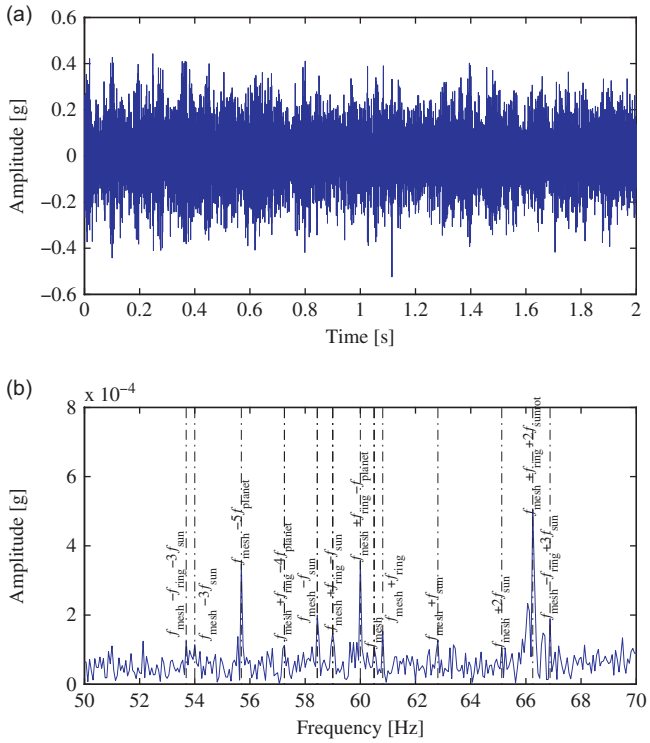

Fig. 6. Industrial planetary gearbox vibration signal: (a) waveform and (b) Fourier spectrum.

Table 3
Characteristic frequencies (Hz).

Meshing frequency	Rotating frequency		Distributed damage			Local damage			
	Sun	Carrier	Planet	Sun	Ring	Planet		Sun	Ring
60.7016	2.5673	0.3994	0.9791	2.1679	0.3994	0.9791	1.9581	6.5037	1.1981

Fig. 5(a) and (b) show the speed and current of the driving motor along with time for more than 6 h. From a long term view of point, both the speed and the current vary dramatically. This implies that the vibration signal would be nonstationary in a long time span. However, from a short time view of point, for example, after the instant labeled by the red dash line, neither the speed nor the current change too much. This allows us to assume the vibration signal in any short time collecting window (16 s only) after the red dash line to be stationary.

Fig. 6 shows the waveform and Fourier spectrum of a signal collected after the red dash line. According to the recorded speed (11.436 Hz at the time collecting the vibration signal), and the gearbox configuration, the characteristic frequencies of the 1st stage planetary gearbox are calculated as listed in Table 3. Since minor distributed damage such as manufacturing errors are inevitable, we label the spectral peaks in terms of the characteristic frequency of distributed gear fault in the Fourier spectrum. In the frequency domain, almost all the prominent spectral peaks appear at the expected characteristic frequencies, such as $f_{\mathrm{mesh}}+f_{\mathrm{ring}}$, $f_{\mathrm{mesh}}+f_{\mathrm{ring}}+2f_{\mathrm{sunrot}}$, $f_{\mathrm{mesh}}\pm kf_{\mathrm{sun}}$, $f_{\mathrm{mesh}}\pm f_{\mathrm{ring}}\pm kf_{\mathrm{sun}}$, and $f_{\mathrm{mesh}}\pm f_{\mathrm{ring}}\pm kf_{\mathrm{planet}}$ (where $k=1,2,\ldots$). This behavior is consistent with the expectation from the signal model and equations for calculating the characteristic frequency of each gear with either local or distributed damage. The presence of these spectral peaks is reasonable because even for normal gearboxes, manufacturing and assembly errors, as well as minor damage are inevitable. These findings illustrate the capability of the proposed method to identify the characteristic frequencies of planetary gearbox vibration signals in industrial applications.

5. Experimental signal analysis

In this section, we use two datasets to validate the performance of spectral analysis in diagnosing planetary gearbox faults according to our theoretical derivations. One is the experimental signals collected from a lab planetary gearbox with

manually created pitting on a planet gear. The other one is the signals from the same gearbox with naturally developed gear wear.

5.1. Experimental specification

Fig. 7 shows the planetary gearbox test rig. We did experiments on the 2nd stage planetary gearbox, for both the manually created damage and the naturally developed fault. Table 4 lists the gear parameters of the 2nd stage planetary gearbox.

For the manual pitting experiments, we introduced pitting of different levels (i.e. baseline, slight, moderate, and severe pitting) to the planet gears inside of the 2nd planetary gearbox. Fig. 8 shows the picture of planet gears with different pitting levels. In each experiment, a planet gear of different pitting level was used, whereas all the other gears were normal. During experiments, the rotating frequency of the input shaft connecting sun gear of the 2nd planetary gearbox

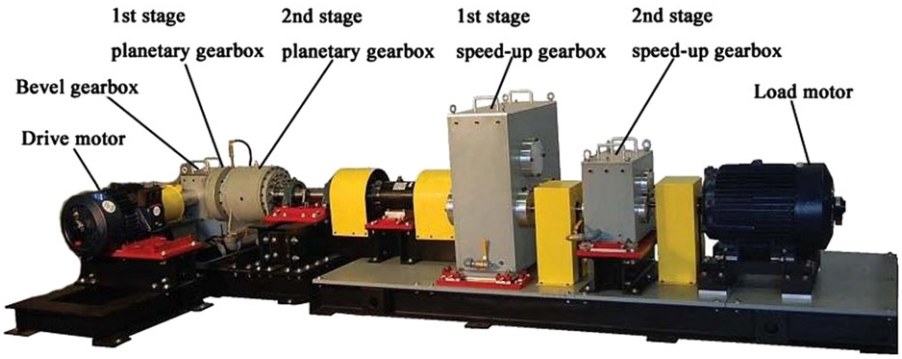

Fig. 7. Planetary gearbox test rig.

Table 4
Gear parameters.

Gear	Sun	Ring	Planet	Number of planets
Number of teeth	19	81	31	4

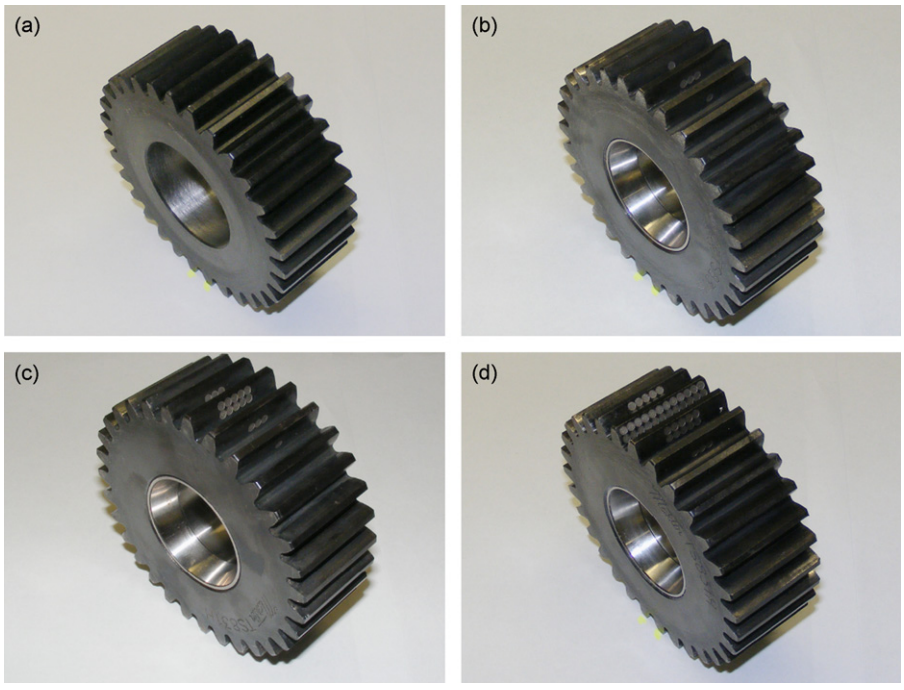

Fig. 8. Planet gears with manually created pitting damage: (a) baseline, (b) slight, (c) moderate and (d) severe.

was set to 0.7778 Hz, and a load of 10,000 lb-in. was applied to the output shaft connecting planet carrier of the 2nd planetary gearbox.

For the naturally developed wear experiment, we used a soft sun gear in the same 2nd planetary gearbox, while the remained gears were all normally hardened. During experiments, the sun gear speed of the 2nd planetary gearbox was also set to 0.7778 Hz, while a heavier load of 25,000 lb-in. was applied to the output shaft connecting planet carrier of the 2nd planetary gearbox. After 98 hours of running, we observed obvious wear on the sun gear. Consequently, the sun gear wear leaded to minor damage on the planet and the ring gears. Fig. 9 shows the gears before and after the experiment. As a result of heat treatment, many scales exist on the gear surface before the experiment, especially on the ring gear surface.

An accelerometer was mounted on the top of the gearbox casing (as shown in Fig. 10), and the vibration signals were collected at a sampling frequency of 10,000 Hz.

According to the planetary gearbox configuration and its running speed, the characteristic frequencies of each gear in the 2nd planetary gearbox are calculated, as listed in Table 5.

5.2. Manual pitting signal analysis

In this section, we firstly validate the performance of spectral analysis in diagnosing planetary gearbox faults according to our theoretical derivation by analyzing the severe planet gear pitting signal, and then illustrate the effectiveness in detecting and locating weak faults by analyzing the moderate and slight planet gear pitting signals.

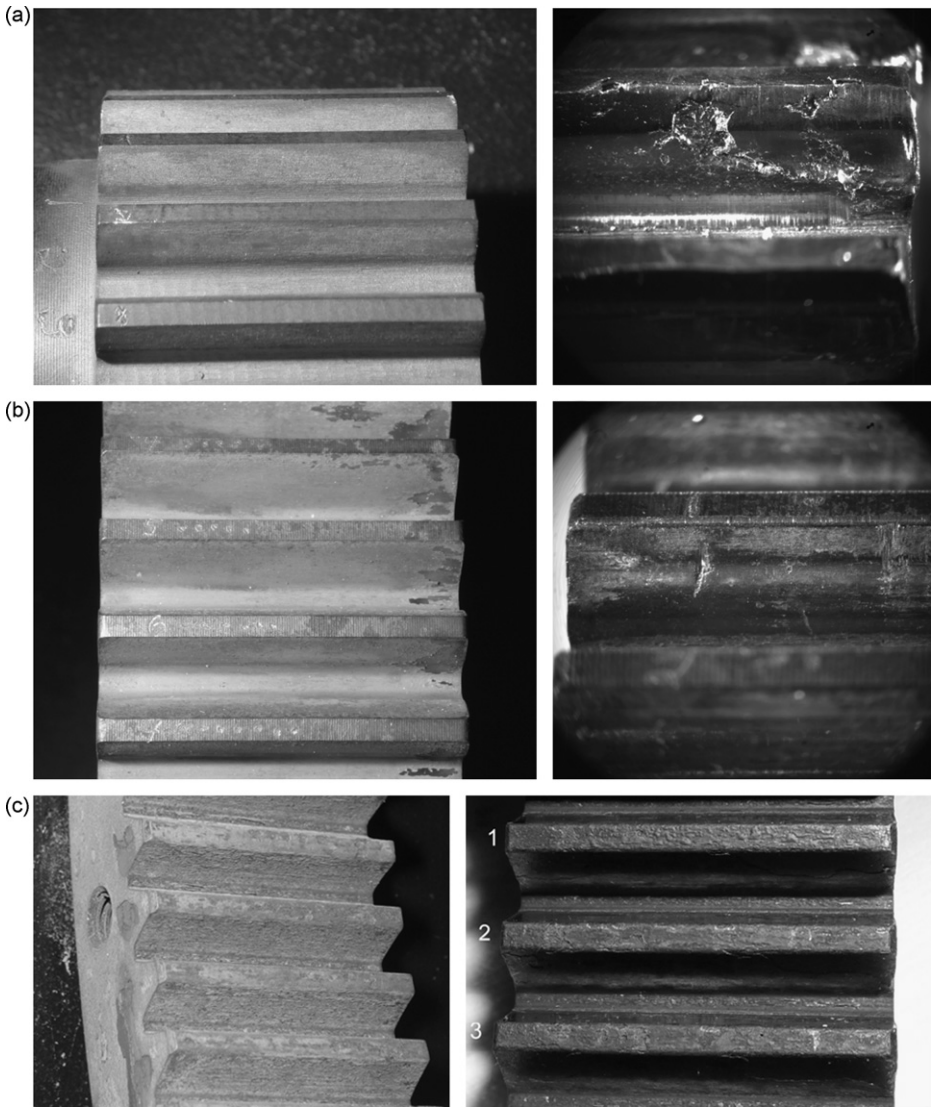

Fig. 9. Gears before (left) and after (right) experiment: (a) sun, (b) planet and (c) ring.

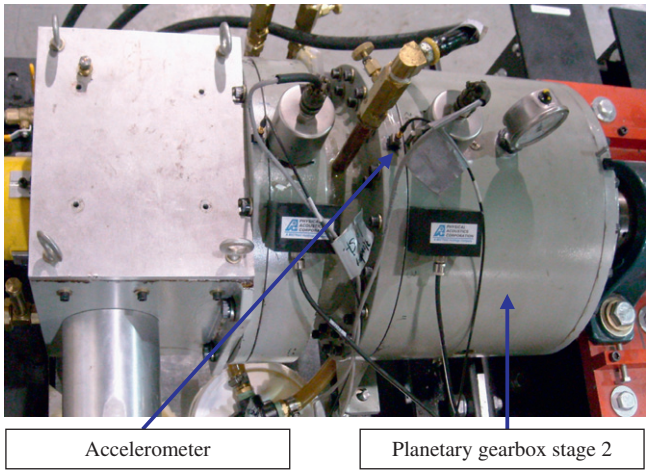

Fig. 10. Sensor location.

Table 5
Characteristic frequencies (Hz).

Meshing frequency	Rotating frequency		Distributed damage			Local damage			
	Sun	Carrier	Planet	Sun	Ring	Planet		Sun	Ring
11.97	0.7778	0.1478	0.3861	0.63	0.1478	0.3861	0.7722	2.52	0.5912

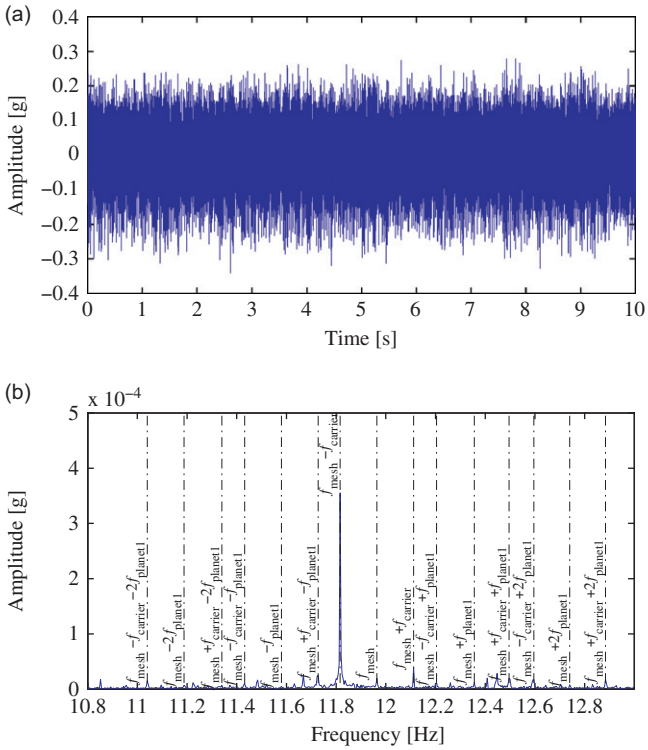

Fig. 11. Baseline signal: (a) waveform and (b) Fourier spectrum.

Figs. 11–14 show both the waveforms and the Fourier spectra of the baseline, severe, moderate and slight pitting signals respectively. The manually created pitting simulates the local gear damage, thus we label the spectral peaks in terms of the characteristic frequency of local gear fault. In all the four cases, the frequency component of $f_{mesh}-f_{carrier}$ is dominant.

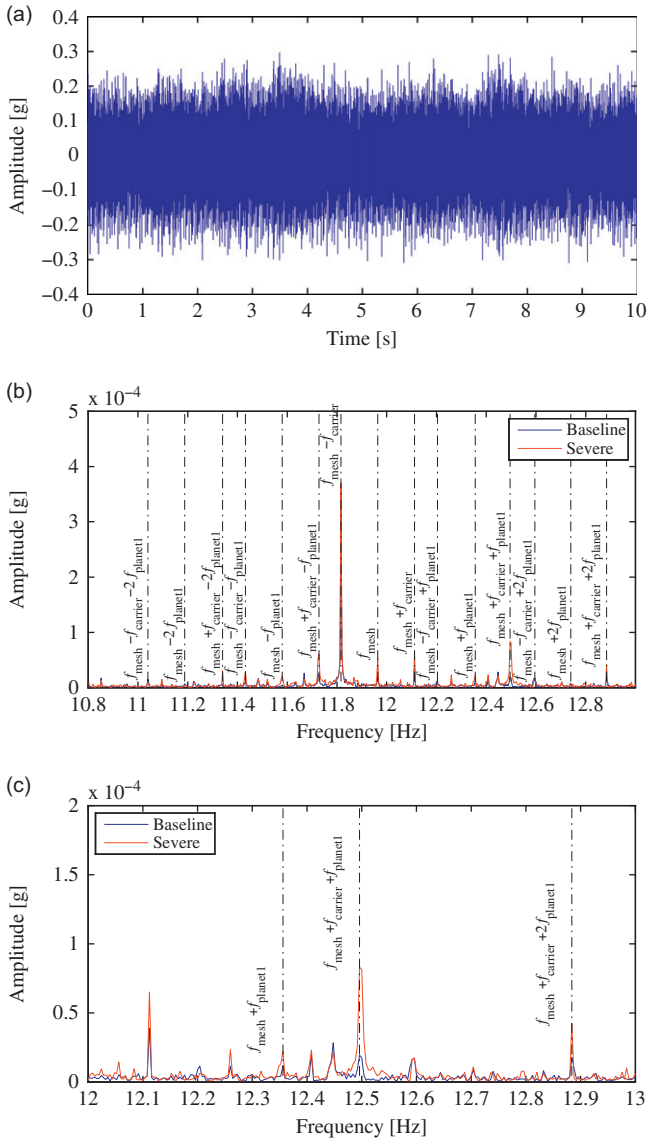

Fig. 12. Severe pitting signal: (a) waveform, (b) Fourier spectrum and (c) zoomed-in Fourier spectrum. (For interpretation of the references to color in this figure, the reader is referred to the web version of this article.)

For the baseline signal, as shown in Fig. 11, some sidebands appear at the frequencies of $f_{\text{mesh}} \pm kf_{\text{planet1}}$ and $f_{\text{mesh}} \pm f_{\text{carrier}} \pm kf_{\text{planet1}}$ (where $k = 1,2,\ldots$), but their amplitudes are not big. The manufacturing errors are inevitable during gear production. They will result in the sidebands even for normal gears. So this does not indicate that planet gears are faulty.

Compared with the baseline signal, the vibration signal of the severe planet gear pitting has a different spectrum, as shown in Fig. 12. The spectral peaks appear at the same frequencies of $f_{\text{mesh}} \pm kf_{\text{planet1}}$ and $f_{\text{mesh}} \pm f_{\text{carrier}} \pm kf_{\text{planet1}}$ (where $k = 1,2,\ldots$) as those of the baseline signal, but most of them have bigger magnitudes. This is consistent with the expectation from Eq. (13): if damage occurs on planet gear tooth, sidebands will appear around three centers, i.e. the meshing frequency f_{mesh} and the meshing frequency minus and plus the planet carrier rotating frequency $f_{\text{mesh}} \pm f_{\text{carrier}}$, with a sideband spacing equal to the characteristic frequency of faulty planet gear f_{planet1} or f_{planet2}. The three center frequencies do not contain any information of damage location, but the sidebands do because they are associated with the characteristic frequency of the faulty gear. So we focus on the sidebands rather than the three centers to detect and locate the gear fault. Fig. 12(c) shows the zoomed-in Fourier spectrum of severe pitting signal. The sidebands at the frequencies of $f_{\text{mesh}}+f_{\text{planet1}}$, $f_{\text{mesh}}+f_{\text{carrier}}+f_{\text{planet1}}$ and $f_{\text{mesh}}+f_{\text{carrier}}+2f_{\text{planet1}}$ (or $f_{\text{mesh}}+f_{\text{carrier}}+f_{\text{planet2}}$), have much bigger peak magnitudes than those of the baseline signal. This indicates the gearbox is faulty, and the pitting occurs on one planet gear. This is consistent with the actual experimental setting.

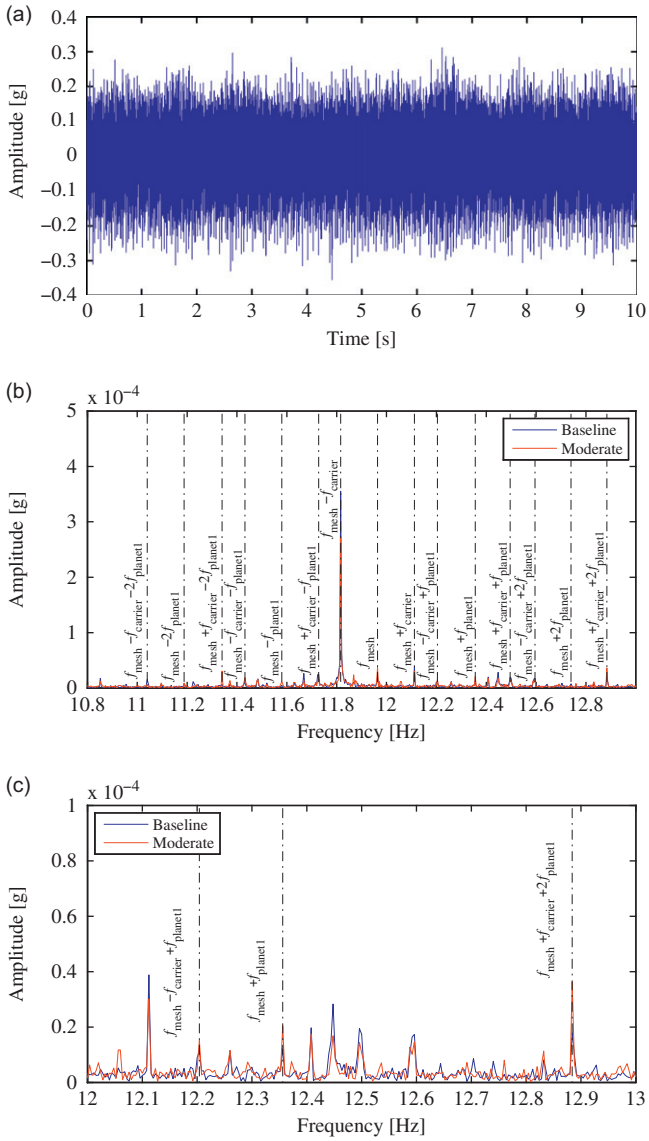

Fig. 13. Moderate pitting signal: (a) waveform, (b) Fourier spectrum and (c) zoomed-in Fourier spectrum. (For interpretation of the references to color in this figure, the reader is referred to the web version of this article.)

For the vibration signal of moderate planet gear pitting, the sidebands at the frequencies of $f_{mesh}-f_{carrier}+f_{planet1}$, $f_{mesh}+f_{planet1}$ and $f_{mesh}+f_{carrier}+2f_{planet1}$ (or $f_{mesh}+f_{carrier}+f_{planet2}$) have bigger magnitudes than those of the baseline signal, as shown in Fig. 13(c). This again indicates the gearbox is faulty, and the pitting occurs on one planet gear.

For the vibration signal of slight planet gear pitting, the sidebands at the frequencies of $f_{mesh}+f_{planet1}$ and $f_{mesh}+f_{carrier}+2f_{planet1}$ (or $f_{mesh}+f_{carrier}+f_{planet2}$) have a little bit bigger magnitudes than those of the baseline, as shown in Fig. 14(c). Though the difference from the baseline signal is not significant, it indicates that the slight pitting occurs on one planet gear.

5.3. Natural wear signal analysis

In this section, we illustrate the effectiveness of spectral analysis in diagnosing naturally developed faults of planetary gearboxes based on our theoretical derivations by analyzing the worn gear signal.

Figs. 15 and 16 show both the waveforms and the Fourier spectra of the baseline and natural wear signals respectively. The naturally developed wear simulates distributed gear damage, thus we label the spectral peaks in terms of the characteristic frequency of distributed gear fault. In both cases, the frequency component of $f_{mesh}-f_{ring}$ is dominant.

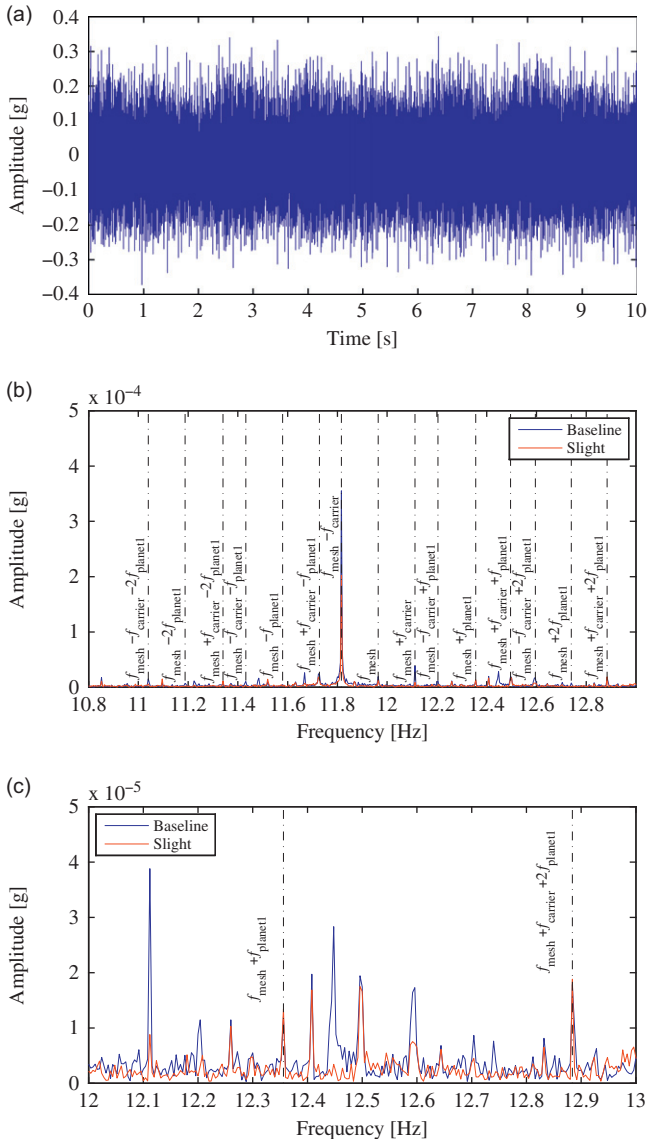

Fig. 14. Slight pitting signal: (a) waveform, (b) Fourier spectrum and (c) zoomed-in Fourier spectrum. (For interpretation of the references to color in this figure, the reader is referred to the web version of this article.)

This phenomenon is similar to those of the manual pitting experimental signals, because the characteristic frequency of the ring gear with distributed damage f_{ring} is equal to the rotating frequency of the planet carrier f_{carrier}.

For the baseline signal, as shown in Fig. 15, some sidebands appear at the frequencies of $f_{\text{mesh}} \pm kf_{\text{ring}}$ and $f_{\text{mesh}} \pm f_{\text{ring}} \pm kf_{\text{planet}}$ (where $k = 1,2,\ldots$), but their amplitudes are not big. The manufacturing errors are inevitable during gear production, for example the residual scales on the gear surface due to heat treatment. They will cause the presence of these sidebands.

For the worn signal, most of the spectral peaks appear at the locations associated with the characteristic frequencies of the planetary gearbox, f_{ring}, f_{planet}, and f_{sun}. They are significantly larger than those of the baseline signal. In particular, prominent spectral peaks appear at the frequencies of $f_{\text{mesh}} - f_{\text{ring}} \pm 4f_{\text{sun}}$, and their magnitudes are significantly larger than those of the baseline (as shown in Fig. 16(c)). These findings imply that all the gears in the planetary gearbox have damage. Even though the naturally developed wear damage mode is far more complicated than the manually created single point local pitting damage, the damage is compound (i.e. both the sun, planet and ring gears have damage), and the planet and ring gear damage are very weak, we can still diagnose the gear faults using spectral analysis based on the theoretical derivations.

All the above analysis results are consistent with the actual experimental setting. This validates our theoretical derivations including both the vibration signal models and the equations for calculating characteristic frequency of each faulty gear in planetary gearboxes.

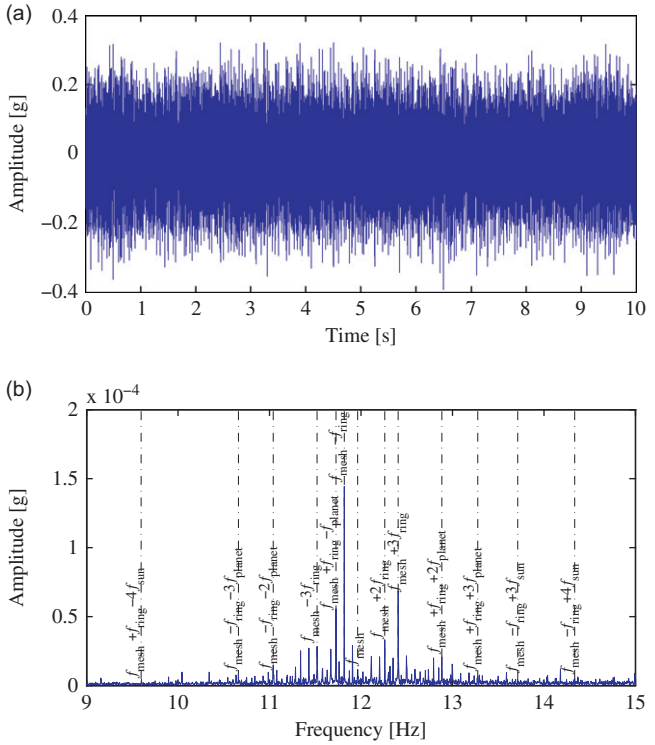

Fig. 15. Baseline signal: (a) waveform and (b) Fourier spectrum.

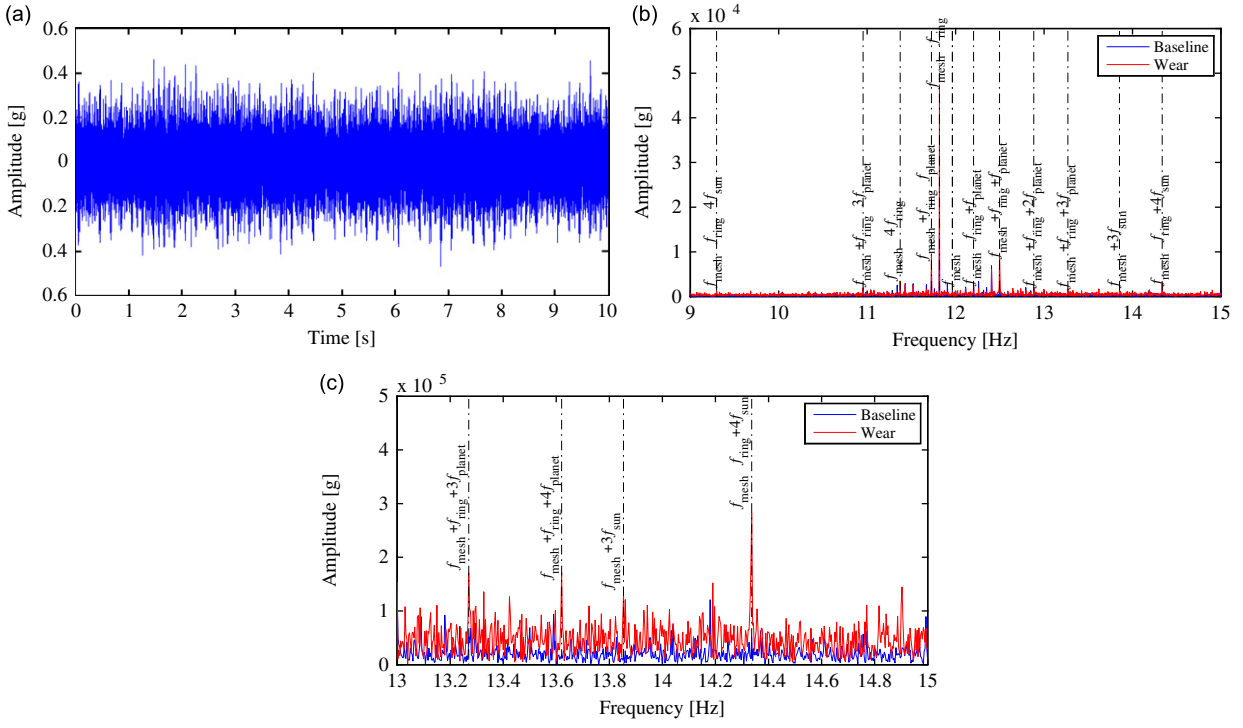

Fig. 16. Wear signal: (a) waveform, (b) Fourier spectrum and (c) zoomed-in Fourier spectrum. (For interpretation of the references to color in this figure, the reader is referred to the web version of this article.)

6. Conclusions

Considering the AMFM effects due to gear fault and time variant working condition, and the signal propagating effect, mathematical models of faulty planetary gearbox vibration signals are given, and their Fourier transform in closed form are derived. The explicit equation for calculating the characteristic frequency of each faulty gear which is important for detecting and locating faults is also deduced. These theoretical derivations provide a theoretical guide for not only detecting but also locating gear faults of planetary gearboxes, and thus hopefully enable the commonly used spectral analysis to be more effective in fault diagnosis of planetary gearboxes. Industrial and lab experimental signal analysis validates the effectiveness of the signal models and the theoretically derived equations of spectral structure and gear characteristic frequency. According to the presence of spectral peaks at the locations of characteristic frequencies in Fourier spectrum, the manually created local gear faults of different levels and the naturally developed gear fault are detected and located.

Acknowledgement

This work is supported by the Natural Sciences and Engineering Research Council of Canada (NSERC), the National Natural Science Foundation of China (51075028, 50705007), and Beijing Natural Science Foundation (3102022). Thanks also go to the anonymous reviewers and the editor for their suggestions and comments, which have helped improve the quality of this paper.

References

[1] P.D. Samuel, D.J. Pines, A review of vibration-based techniques for helicopter transmission diagnostics, *Journal of Sound and Vibration* 282 (2005) 475–508.
[2] P.D. McFadden, A technique for calculating the time domain averages of the vibration of the individual planet gears and the sun gear in an epicyclic gearbox, *Journal of Sound and Vibration* 144 (1991) 163–172.
[3] P.D. McFadden, Window functions for the calculation of the time domain averages of the vibration of the individual planet gears and sun gear in an epicyclic gearbox, *Journal of Vibration and Acoustic* 116 (1994) 179–187.
[4] P.D. Samuel, D.J. Pines, Vibration separation methodology for planetary gear health monitoring, *Proceeding of SPIE* 3985 (2000) 250–260.
[5] W.J. Williams, E.J. Zalubas, Helicopter transmission fault detection via time–frequency, scale and spectral methods, *Mechanical Systems and Signal Processing* 14 (2000) 545–559.
[6] P.D. Samuel, D.J. Pines, Constrained adaptive lifting and the CAL4 metric for helicopter transmission diagnostics, *Journal of Sound and Vibration* 319 (2009) 698–718.
[7] W. Bartelmus, R. Zimroz, Vibration condition monitoring of planetary gearbox under varying external load, *Mechanical Systems and Signal Processing* 23 (2009) 246–257.
[8] W. Bartelmus, R. Zimroz, A new feature for monitoring the condition of gearboxes in non-stationary operation conditions, *Mechanical Systems and Signal Processing* 23 (2009) 1528–1534.
[9] P.D. McFadden, J.D. Smith, An explanation for the asymmetry of the modulation sidebands about the tooth meshing frequency in epicyclic gear vibration, *Proceedings of the Institution of Mechanical Engineers* 199 (C1) (1985) 65–70.
[10] J. McNames, Fourier series analysis of epicyclic gearbox vibration, *Journal of Vibration and Acoustics-Transactions of the ASME* 24 (2002) 150–152.
[11] M. Mosher, Understanding vibration spectra of planetary gear systems for fault detection, *Proceedings of ASME Design Engineering Technical Conferences*, 2003, pp. 1–8.
[12] M. Inalpolat, A. Kahraman, A theoretical and experimental investigation of modulation sidebands of planetary gear sets, *Journal of Sound and Vibration* 323 (2009) 677–696.
[13] M. Inalpolat, A. Kahraman, A dynamic model to predict modulation sidebands of a planetary gear set having manufacturing errors, *Journal of Sound and Vibration* 329 (2010) 371–393.
[14] R.B. Randall, A new method of modeling gear faults, *Journal of Mechanical Design* 104 (1982) 259–267.
[15] P.D. McFadden, Detecting fatigue cracks in gears by amplitude and phase demodulation of the meshing vibration, *Journal of Vibration Acoustics Stress and Reliability in Design-Transactions of the ASME* 108 (1986) 165–170.
[16] J. Lin, M.J. Zuo, Extraction of periodic components for gearbox diagnosis combining wavelet filtering and cyclostationary analysis, *Journal of Vibration and Acoustics* 126 (2004) 449–451.
[17] X. Fan, M.J. Zuo, Gearbox fault detection using Hilbert and wavelet packet transform, *Mechanical Systems and Signal Processing* 20 (2006) 966–982.
[18] Z. Feng, F. Chu, Application of atomic decomposition to gear damage detection, *Journal of Sound and Vibration* 302 (2007) 138–151.
[19] S. Wu, M.J. Zuo, A. Parey, Simulation of spur gear dynamics and estimation of fault growth, *Journal of Sound and Vibration* 317 (2008) 608–624.
[20] Z. Feng, M.J. Zuo, Fulei Chu, Application of regularization dimension to gear damage assessment, *Mechanical Systems and Signal Processing* 24 (2010) 1081–1098.
[21] Z. Feng, M.J. Zuo, R. Hao, F. Chu, Gear damage assessment based on cyclic spectral analysis, *IEEE Transactions on Reliability* 60 (2011) 21–32.
[22] M. Abramowitz, I.A. Stegun, Handbook of Mathematical Functions With Formulas, Graphs, and Mathematical Tables, Dover, New York, NY, 1972.